Dalton Transactions

ROYAL SOCIETY OF CHEMISTRY

PAPER

View Article Online
View Journal | View Issue

Cite this: *Dalton Trans.*, 2022, **51**, 13376

Understanding the role of flux, pressure and temperature on polymorphism in ThB_2O_5†

Yucheng Hao, [a] Gabriel L. Murphy, *[b] Philip Kegler,[b] Yan Li, [c] Piotr M. Kowalski, [d,e] Simon Blouin,[f,g] Yang Zhang,[a] Shuao Wang, [h] Lars Robben,[i,j] Thorsten M. Gesing [i,j] and Evgeny V. Alekseev *[k]

A novel polymorph of ThB_2O_5, denoted as β-ThB_2O_5, was synthesised under high-temperature high-pressure (HT/HP) conditions. *Via* single crystal X-ray diffraction measurements, β-ThB_2O_5 was found to form a three-dimensional (3D) framework structure where thorium atoms are ten-fold oxygen co-ordinated forming tetra-capped trigonal prisms. The only other known polymorph of ThB_2O_5, denoted α, synthesised herein using a known borax, B_2O_3–$Na_2B_4O_7$, high temperature solid method, was found to transform to the β polymorph when exposed to conditions of 4 GPa and ~900 °C. Compared to the α polymorph, β-ThB_2O_5 has smaller molar volume by approximately 12%. Exposing a mixture of the α and β polymorphs to HT/HP conditions *ex situ* further demonstrated the preferred higher-pressure phase being β, with no α phase material being observed *via* Rietveld refinements against laboratory X-ray powder diffraction (PXRD) measurements. *In situ* heating PXRD measurements on α-ThB_2O_5 from RT to 1030 °C indicated that α-ThB_2O_5 transforms to the β variant at approximately 900 °C *via* a 1st order mechanism. β-ThB_2O_5 was found to exist only over a narrow temperature range, decomposing above 1050 °C. *Ab initio* calculations using density functional theory (DFT) with the Hubbard U parameter indicated, consistent with experimental observations, that β is both the preferred phase at higher temperatures and high pressures. Interestingly, it was found by switching from B_2O_3–$Na_2B_4O_7$ to H_3BO_3–Li_2CO_3 flux using consistent high temperature solid state conditions for the synthesis of the α variant, β-ThB_2O_5 could be generated. Comparison of their single crystal measurements showed this was identical to that obtained from HT/HP conditions.

Received 5th April 2022,
Accepted 8th August 2022

DOI: 10.1039/d2dt01049f

rsc.li/dalton

[a]*School of Energy Materials and Chemical Engineering, Hefei University, Hefei 230000, China. E-mail: haoyco@hfuu.edu.cn*
[b]*Institute of Energy and Climate Research (IEK-6), Forschungszentrum Jülich GmbH, 52428 Jülich, Germany. E-mail: murphy@fz-juelich.de*
[c]*State Key Laboratory of Optoelectronic Materials and Technologies, School of Materials Science and Engineering, Sun Yat-sen (Zhongshan) University, Guangzhou, 510275, PR China*
[d]*Institute of Energy and Climate Research (IEK-13), Forschungszentrum Jülich GmbH, 52428 Jülich, Germany*
[e]*JARA Energy & Center for Simulation and Data Science (CSD), Jülich, Germany*
[f]*Department de Physique, University of Montreal, Montreal, QC H3C 3J7, Canada*
[g]*Department of Physics and Astronomy, University of Victoria, Victoria, BC V8P 5C2, Canada*
[h]*School for Radiological and Interdisciplinary Sciences (RAD-X) and Collaborative Innovation Center of Radiation Medicine of Jiangsu Higher Education Institutions, Soochow University, Suzhou 215123, China*
[i]*University of Bremen, Institute of Inorganic Chemistry and Crystallography, D-28359 Bremen, Germany*
[j]*University of Bremen, MAPEX Center for Materials and Processes, D-28359 Bremen, Germany*
[k]*Institute of Energy and Climate Research (IEK-9), Forschungszentrum Jülich GmbH, 52428 Jülich, Germany. E-mail: e.alekseev@fz-juelich.de*

† Electronic supplementary information (ESI) available: X-ray crystallographic files in CIF format, SEM and EDS measurement, selected bond distances and angles, TG-DSC curves, and vis-IR spectroscopy. CCDC 2106445. For ESI and crystallographic data in CIF or other electronic format see DOI: https://doi.org/10.1039/d2dt01049f

1. Introduction

Traditional interest in thorium chemistry has been somewhat overshadowed by its f-block sister uranium,[2,3] however contemporary studies have unravelled significant applications and properties in the context of advanced functional material development, reinvigorating focus in the most naturally abundant actinide element.[4–6] Examples of such successes can be seen in nuclear waste separation technology,[7a] radiation detection[7b] and also MOF development.[7c] In these, the chemical advantages derived from the typically tetravalent Th cation, as opposed to its higher actinide counterparts (U, Np, Pu), relate to its ability to adopt a relatively more spherical chemical environment whilst retaining somewhat f-block character.[8] This allows for the construction of unique higher dimensional structures than those typically found for instance in uranyl compounds. Accordingly, together with property measurements and applications, inorganic chemists have shifted their attention towards deriving facile synthesis routes to unlock novel thorium phases and study their structural properties.

Since the exceptional Tc ion-exchangeable thorium borate, NDTB-1 ($ThB_5O_6(OH)_6$ $BO(OH)_2{\cdot}2.5H_2O$) was first reported in

2010, interest in thorium borate synthesis has grown.[9] However, surprisingly only a few thorium borates without additional countercations have been reported.[1,9,10] Prior to NDTB-1, Cousson and Gasperin in 1991 reported the first example of a thorium borate, ThB_2O_5 (denoted hereon as α-*phase*), which was obtained through high-temperature flux synthesis.[1] It consists of a 3D thorium borate framework structure, in which thorium–thorium stacking sequences exist with a diamond packing motif forming a 3D thorium-network. B_2O_5 dimers edge share with thorium polyhedra and fill the voids of the Th-cation framework along the [−101] direction. NDTB-1 was originally synthesised using a low-temperature boric acid flux method in which this thorium borate is constructed from crown-like $B_{10}O_{24}$ groups and twelve-fold coordinated thorium ions. These groups form a porous super-tetrahedral 3D thorium-borate framework. The super-tetrahedra cationic framework in NDTB-1 contributes to its superb anion exchange properties. Hinteregger *et al.* prepared the third member of the thorium borates system, ThB_4O_8, which was synthesised under extreme conditions (5.5 GPa/1100 °C) through a high temperature/high pressure (HT/HP) method.[10] Its structure is based on 2D polyborate layers composed of corner-sharing BO_4 tetrahedra where the ten-fold coordinated thorium cations are located in the interlayer space. Currently, there are no further reports of other thorium borates than the three described.

With the motivation of understanding the structural chemistry and behavior of thorium borates under variable conditions a part of our general focus on exploring chemistry of actinide compounds,[2–9] we have examined the Th–B–O system towards expanding knowledge of it and ascertaining fundamental chemical insight. Herein, we report a new polymorph in the ThB_2O_5 family, β-ThB_2O_5, from HT/HP conditions and examine the temperature and pressure relationship it has to the only other reported polymorph,[1] α, using experimental and theoretical methods. Interestingly although β-ThB_2O_5 is found to be the preferred higher pressure and temperature phase, relative to α-ThB_2O_5, it can also be accessed through careful choice of flux under ambient pressure solid state high temperature conditions. The synthetic conditions, structural chemistry and topology, phase relationship and phase decomposition process, thermodynamics stability, theoretical analysis as well as Raman and IR spectra of both polymorphs are discussed.

2. Experiment section

2.1 Materials and methods

Thorium nitrate $Th(NO_3)_4{\cdot}5H_2O$ (International Bioanalytical Industries, Inc.), Lithium carbonate Li_2CO_3 (Alfa-Aesar, 99.9%), Boric acid H_3BO_3 (Alfa-Aesar, 99.9%), Sodium Tetraborate $Na_2B_4O_7$ (Alfa-Aesar, 99.5%), Boron Oxide B_2O_3 (Alfa-Aesar, 99.5%).

2.2 Synthesis

2.2.1 α-ThB_2O_5 – high temperature solid state flux growth.[1] A mixture of ThO_2, $Na_2B_4O_7$ and B_2O_3 at a molar ratio of 1/2/10, was heated in the air at ∼1200 °C for 15 hours, and then cooled down to room temperature slowly (5 °C h^{-1}). After washing with boiling water, homogeneous product, composed of prism colourless transparent crystals of monoclinic α-ThB_2O_5 were prepared.[1] A nearly pure polycrystalline sample of α-ThB_2O_5 was prepared by reacting a mixture of Th $(NO_3)_4{\cdot}5H_2O$ (0.302 g, 0.53 mmol) and H_3BO_3 (0.073 g, 1.18 mmol) with a molar ratio of 1 : 2.2 at ∼780 °C for 36 hours. The samples were then washed with boiled water and ethanol several times to eliminate impurities.

2.2.2 β-ThB_2O_5 – high pressure/high temperature. Single crystals of monoclinic β-ThB_2O_5 were obtained using a HT/HP method. For the HT/HP method a piston cylinder module of a Voggenreiter LP 1000-540/50 device was used. The starting chemicals of $Th(NO_3)_4{\cdot}5H_2O$ (0.115 g, 0.19 mmol) and B_2O_3 (0.0795 g, 1.15 mmol) with a ratio of Th : B = 1 : 6 were used. All the reagents were thoroughly ground in an agate mortar and then transferred to a small platinum crucible of 4 mm diameter and 7 mm height which was sealed. A pressure of 4.0 GPa was applied within 0.5 hours before heating (cold piston in). The reaction mixtures were kept at 4.0 GPa for the whole experimental run. The temperature was increased up to 1000 °C in 0.5 hours. The temperature was held at 1000 °C for 6 hours then slowly cooled down to 700 °C with a rate of 5 °C h^{-1}. The following next step cooled the assembly down to 450 °C at a rate of 10 °C h^{-1} followed by quenching to room temperature and subsequent pressure release. For extracting the resulting products, the platinum crucible was broken. Colorless pallet shaped crystals were isolated.

2.2.3 β-ThB_2O_5 – high temperature solid state flux growth. For high temperature flux synthesis of β-ThB_2O_5, Th $(NO_3)_4{\cdot}5H_2O$ (0.105 g, 0.18 mmol), H_3BO_3 (0.0618 g, 1.00 mmol) and Li_2CO_3 (0.0182 g, 0.25 mmol) were mixed in a mortar and grinded thoroughly, then transferred into a platinum crucible. The mixture was held in a box furnace at 450 °C for 1 hour to decompose the thorium nitrate and boric acid. Then the temperature was increased to 970 °C for 5 hours until the homogeneous melt was formed. After this, the melt was cooled down to 700 °C at a rate of 5 °C h^{-1} and then cooled down to room temperature with a cooling rate of 10 °C h^{-1}. The resulting product was washed with hot water to remove the excess of boric acid. Large colorless block shaped crystals of β-ThB_2O_5 were obtained.

A nearly pure polycrystalline sample of β-ThB_2O_5 was prepared quantitatively by reacting a mixture of $Th(NO_3)_4{\cdot}5H_2O$ (0.306 g, 0.54 mmol) and H_3BO_3 (0.090 g, 1.45 mmol) with a molar ratio of 3 : 8 and exposed to conditions of 4 GPa/900 °C for 36 hours. The samples were then washed with boiling water several times to eliminate impurities. Energy dispersive X-ray spectroscopy (EDS) elemental analysis on several single crystals gave an average molar ratio of Th : O = 1 : 5.35 for β-ThB_2O_5, which is in good agreement with those obtained from single crystal X-ray diffraction studies (Fig. S1†).

2.3. *Ex situ* and *in situ* experimentation on α and β phases

2.3.1 High-temperature/high-pressure treatment of α- and β-ThB_2O_5 mixture. To understand how the pressure influence

the polymorphism we exposed both polymorphs to high-pressure conditions using the piston cylinder module of a Voggenreiter LP 1000-540/50. The starting material contained a mixture of β-ThB_2O_5 and α-ThB_2O_5 (0.2055 g) with ratio about 15% to 85%, respectively. The mixture was thoroughly ground, pressed and then sealed in a platinum crucible. The pressure was raised to 4.0 GPa within 0.5 hours and then the mixture was kept under 4.0 GPa for the whole experimental run. The temperature was increased up to 900 °C in 0.5 hours, after the pressure was stabilised at 4.0 GPa. The temperature was held at 900 °C for 6 hours and then cooled down to 500 °C at a rate of 10 °C h^{-1} followed by quenching to room temperature. The pressure was released after sample cooling in half an hour. For extracting the resulting products, the platinum crucible was carefully opened. The colourless powder was isolated and characterised with PXRD diffraction (Fig. S2†).

2.3.2 Thermal analysis. The thermal behavior of the dried powder of β-ThB_2O_5 up to 1200 °C was studied by differential scanning calorimetry (DSC) analysis coupled with thermogravimetry (TG) in air at a heating rate of 10 °C min^{-1} using a Netzsch STA 449C Jupiter apparatus. The sample (20.5 mg) was loaded in a platinum crucible, which was covered by a platinum cover. During the measurements a constant air flow of 20–30 mL min^{-1} was applied.

2.4 Analysis crystallographic study and X-ray powder diffraction

2.4.1 Single crystal diffraction. Diffraction data for β-ThB_2O_5 were collected on an Agilent Technologies SuperNova diffractometer with Mo-Kα radiation (λ = 0.71073 Å) at room temperature. All data sets were corrected for Lorentz and polarisation factors as well as for absorption by the multi-scan method.[11] Structure of the compound was solved by direct method and refined with a full-matrix least-squares fitting on F^2 by SHELX.[11] No higher symmetry elements were found after checking using the PLATON with the ADDSY Malgorithms.[11] Crystallographic data and structural refinement information for this β-ThB_2O_5 is summarised in Table 1. The crystal chemical calculations for both ThB_2O_5 phases were performed with TOPOS 4.0 Professional software.[11] Further information for selected bond distances and angles are listed in Table S1.†

2.4.2 *In situ* high temperature X-ray diffraction. High-temperature X-ray powder diffraction data were collected on a Panalytical MPD powder diffractometer (Cu-radiation, Ni-filter, X'Celerator detector, Anton Paar HTK1200N heating chamber) with Bragg–Brentano geometry. Experiments were performed in the range from 27 °C to 1027 °C for pure α-ThB_2O_5 (see Fig. 5) and 27 °C to 1147 °C for the mixture of α-/β-ThB_2O_5 (see Fig. S5†) with a step of 20 °C. Each diffraction pattern was recorded with a step size of 0.0167°. The pure phase α-ThB_2O_5 data was analysed *via* sequential refinements with the Le Bail method, results are giving in Fig. S3 and S4.†

2.4.3 PXRD analysis. Powder X-ray diffraction data (PXRD) was measured on a Bruker-AXS D4 Endeavor diffractometer, 40 kV/40 mA, in Bragg–Brentano geometry. The diffractometer is equipped with a copper X-ray tube and a primary nickel filter producing CuKα radiation. A linear silicon strip LynxEye detector (Bruker-AXS) was used. Data[12] were recorded in the range of 2θ = 10–80° with 5 s/step and a step width of 0.02°. The aperture of the fixed divergence slit was set to 0.2 mm and the receiving slit with 8.0 mm, respectively. The discriminator of the detector was set to an interval of [0.16–0.25 V]. Collected data for the α-ThB_2O_5/β-ThB_2O_5 mix pre- and post-HT/HP treatment were analysed using the Rietveld refinement method using the program GSAS-II[13] Starting models were used derived from SC-XRD structural solutions where the peak shapes were modelled using a pseudo-Voigt function and the background was estimated using a 6 term shifted Chebyschev function. The scale factor, detector, zero point, lattice parameters, atomic coordinates and atomic displacement parameters for cations and phase fractions were refined together with the peak profile parameters.

Table 1 Crystal data and structure refinement details for β-ThB_2O_5 and Crystal Data for α-ThB_2O_5[1]

Compound	β-ThB_2O_5	α-ThB_2O_5[1]
FW	333.66	333.66
Space group	$P2_1/m$	$C2/c$
a (Å)	4.2535(2)	11.545(3)
b (Å)	6.8733(3)	6.937(2)
c (Å)	6.3242(3)	10.263(3)
α (°)	90	90
β (°)	106.316(5)	101.5(3)
γ (°)	90	90
V (Å^3)	177.445(14)	805.44
Z	2	8
λ (Å)	0.71073	
F(000)	280	
D_c (g cm^{-3})	6.245	5.500
GOF on F^2	0.851	
R_1[a]	0.0261	
wR_2[b]	0.0609	

[a] $R_1 = \Sigma||F_o| - |F_c||/\Sigma|F_o|$, [b] $wR_2 = \{\Sigma w[(F_o)^2 - (F_c)^2]^2/\Sigma w[(F_o)^2]^2\}^{1/2}$

2.5 Scanning electron microscopy (SEM)/energy-dispersive X-ray spectroscopy (EDS) analysis

Scanning electron microscopy image and energy-dispersive X-ray spectroscopy (SEM/EDS) was collected on a FEI Quanta 200F Environment Scanning Electron Microscope with a low-vacuum mode at 0.6 mbar. SEM/EDS results were given as ESI (Fig. S1†).

2.6 Raman and IR spectroscopy

Unpolarised Raman spectra were measured with a Horiba LabRAM HR spectrometer using a Peltier cooled multichannel CCD detector. An objective lens with a 50× magnification was linked to the spectrometer, allowing the analysis of samples as small as 2 μm in diameter. The samples were in the form of single crystals. The incident radiation was produced by a He–Ne laser line at a power of 17 mW (λ = 632.8 nm). The focal length of the spectrometer was 800 mm, and an 1800 gr mm^{-1} grating was used. The spectral resolution was approximately 1 cm^{-1} with a slit of 100 μm. The spectrum was recorded in

the range of 100–4000 cm^{-1}. Infrared (IR) spectrum was measured using polycrystalline samples mixed with KBr powder, with FT-IR spectrometer Bruker Equinox 55 at room temperature.

2.7 Bond-valence analysis

As a common method in coordination chemistry to evaluate the oxidation states of atoms, BVS of all atoms in the thorium borate phase were calculated and agree well with corresponding formal values of oxidation states. The bond-valence parameters for Th(IV)–O and B(III)–O were used according to Brese and O'Keeffe.[14]

2.8 *Ab initio* calculations

The computational studies of the ThB_2O_5 system were performed with density functional theory (DFT) method using Quantum-ESPRESSO[15] simulation package. Because we are interested in good computations of structures of considered materials we applied PBEsol exchange/correlation functional,[16] which was successfully applied in the previous studies of *an*-bearing systems.[8,17] The core electrons of the constituent atoms were modeled with ultrasoft pseudopotentials[18] and the $6s^26p^66d^27s^2$ electrons of thorium atom were computed explicitly. Based on previous experience with computing Th-bearing systems, we selected 50Ryd as plane-wave energy cutoff.[19]

The α- and β-ThB_2O_5 structures were modeled with 16 and 64 atoms contained supercells and the calculations were performed on the 6 × 4 × 4 and 2 × 4 × 3 Methfessel–Paxton *k*-points grids.[20] The calculations of phonons and vibrational entropy contributions to Gibbs free energies were performed with the density functional perturbation theory using PHONON and DYNMAT packages of the Quantum-ESPRESSO code.

3.1 Results and discussion

3.1 Syntheses

β-ThB_2O_5 was successfully synthesised *via* a HT/HP method with conditions of 4 GPa and temperature of 1000 °C. It was further found that β-ThB_2O_5 could be successfully synthesised through a high temperature flux method with H_3BO_3–Li_2CO_3. It was found that by switching the fluxes from H_3BO_3–Li_2CO_3 to B_2O_3–$Na_2B_4O_7$ the known α polymorph[1] could be obtained. It is pertinent that we used different initial reactants (Th$(NO_3)_4{\cdot}5H_2O$/Li_2CO_3/H_3BO_3) for preparation of β-ThB_2O_5 compared to (ThO_2/$Na_2B_4O_7$/B_2O_3) the synthesis of α-ThB_2O_5. It was found that by heating a sample α-ThB_2O_5 between 800 to 1200 °C, β-ThB_2O_5 could be obtained indicating that α transforms to β with increasing temperature. If a mixture of α-ThB_2O_5 and β-ThB_2O_5 or a single sample of α-ThB_2O_5 was exposed to HT/HP conditions of 4 GPa, ~900 °C, only the β polymorph with some additional minor ThO_2 was obtained. This indicates that a pressure induced phase transition occurs from α to β-ThB_2O_5 with increasing pressure which is logical because β-phase has significantly higher density. A difference in volume of ~12 $Å^3$, at P = 4 GPa, corresponds to ΔVP = 29 kJ mol^{-1}, which is larger than the difference in the free energy calculated between α and β phases (Table 2) from *ab initio* calculations. Hinteregger *et al.* reported the synthesis of ThB_4O_8, under similar HT/HP conditions to that of the present investigation (5.5 GPa, 1000 °C).[10] The density of ThB_4O_8 (5.970 g cm^{-3}) is larger than that of α-ThB_2O_5 (5.50 g cm^{-3}) and smaller compared to that of β-ThB_2O_5 (6.245 g cm^{-3}).

Table 2 The difference in Gibbs free energy between α-ThB_2O_5 and β-ThB_2O_5 phases. The energies are reported in kJ mol^{-1}

	ΔU (0 K)	ΔU + ZPE (0 K)	ΔG (300 K)	ΔG (1000 K)	ΔG (1200 K)	ΔG (1500 K)
$\Delta G = G(\beta) - G(\alpha)$	34.4	31.8	28.1	12.6	8.1	1.5

3.2 Structural description of β-ThB_2O_5 and comparison to α-ThB_2O_5

Structural refinements against single crystal X-ray diffraction data reveal that novel β-ThB_2O_5 crystallises in the monoclinic space group $P2_1/m$. It consists of one crystallographically independent Th, two B and four O atoms. The 3D framework of β-ThB_2O_5 is based on 1D B chains and 2D Th layers (see Fig. 1). In the structure of β-ThB_2O_5, B(1) atoms are existing as $B(1)O_4$ tetrahedra and B(2) atoms are forming $B(2)O_3$ planar triangles. $B(1)O_4$ tetrahedra and $B(2)O_3$ triangles are connected with each other through corner sharing, forming a 1D zigzag B–O chain along the *a*-axis (see Fig. 1b). The oxo-borate fragments are polymerising into 2D layers in the structure of the phases from the family of closely related compounds AB_2O_5 (A = Zr, Hf).[21,22] B atoms occur only as BO_4 tetrahedra within the structures of AB_2O_5 (A = Zr, Hf).

In β-ThB_2O_5, two BO_4 tetrahedra are corner sharing with two ThO_{10} polyhedra, forming four-membered ring channels along the *a*-axis. B–O bond lengths in $B(1)O_4$ tetrahedra are found to range from 1.455(7) Å to 1.472(11) Å. The O–B(1)–O bond angles are in the range of 105.8(7)°–113.1(5)°. The B–O bond distances in $B(2)O_3$ are in the range from 1.356(11) Å to 1.390(11) Å. The O–B(2)–O bond angles are in the range of 114.2(7)°–127.4(8)°, which are consistent with the borates reported previously (see Table S2†).[23]

The Th atoms in β-ThB_2O_5 are coordinated by eight shorter and two longer Th–O bonds giving a ten-fold oxygen coordination, resulting in ThO_{8+2} tetra-caped trigonal prisms (Fig. 2 and Fig. S6). The shorter eight Th–O bonds range in length from 2.302(5) Å to 2.583(6) Å, whereas the additional longer two Th-O bonds are 3.067(6) Å. These ThO_{8+2} polyhedra are edge and face sharing with each other forming 2D sheets parallel to the *ab*-plain (see Fig. 1c). The zigzag B–O chains further link the 2D Th-based sheets, through corner (BO_4), edge (BO_3), and face (BO_4) sharing, and form the 3D Th borate framework (see Fig. S7†). In the 3D thorium borate framework, a four-membered ring channel can be observed along the *a*-axis. The size of this channel is ~4.5 Å × 3.5 Å (distances are

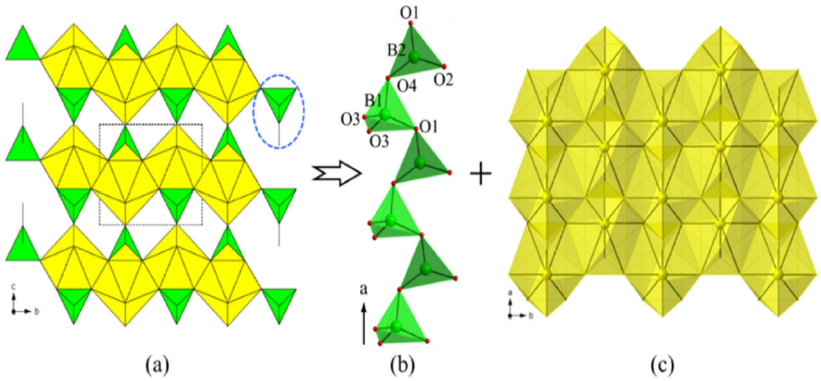

Fig. 1 Polyhedral representation of β-ThB_2O_5 structure. The 3D thorium borate structure along the *a*-axis (a), a 1D boron–oxygen chain along the *a*-axis (b), a 2D thorium layer on *ab*-plane (c). Thorium polyhedra, BO_3 triangles and BO_4 tetrahedra are shown in yellow and green, oxygen atoms are shown in red, respectively.

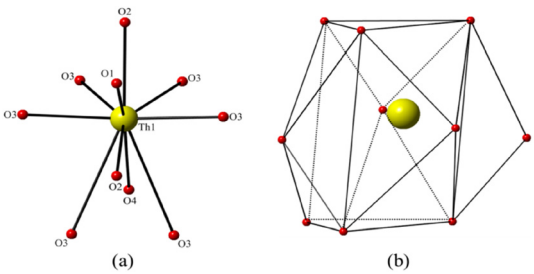

Fig. 2 (a) The oxygen coordination environment of thorium cation with ball and stick mode, (b) the four caped trigonal prismatic shape of thorium polyhedra for β-ThB_2O_5. Th and O atoms are shown as yellow and red, respectively.

between two opposite O–O atoms) (see Fig. S8†). BVS calculations indicate that Th cations are tetravalent with a value of 3.97. The BVS values suggest that the B cation is trivalent with B(1) and B(2) BVS of ~3.07 and ~2.97, respectively.[14]

Contrasting the structures of α-ThB_2O_5 and β-ThB_2O_5, both possess 3D framework structures, which are composed of two independent B and one Th atoms per unit cell. However, B atoms are only presented as BO_3 triangles in the α phase.

In the structure of α-ThB_2O_5, two BO_3 triangles are corner sharing linked forming isolated B_2O_5 dimers. Each BO_3 triangle is corner sharing with two and edge sharing with one Th polyhedra, forming BTh_3 fragments with linear geometry (see Fig. S9†). In the structure of β-ThB_2O_5, as described above, B(1)O_4 tetrahedra and B(2)O_3 triangles are corner sharing and form 1D zigzag chains. Within the 1D B–O chains, the two shortest B–B distances are 2.489(3) Å and 2.594(1) Å, respectively. For comparison, the shortest B(1)–B(2) distance in the structure of α-ThB_2O_5 is 2.445(1) Å. Th cations are eight-fold coordinated in the structure of α-ThB_2O_5 and exist as distorted one-caped pentagonal bipyramids. These ThO_8 distorted one-caped pentagonal bipyramids are edge sharing with each other, forming a 3D Th–O framework. Each Th cation is connected to four other Th cations in a diamond packing mode in the structure of α-ThB_2O_5. The four shortest Th–Th distances are ranging from 4.071(1) Å to 4.131(3) Å in the structure of α-ThB_2O_5. There are seven neighboring Th cations with Th-Th distances ranging from 3.965(5) Å to 4.411(2) Å in the structure of β-ThB_2O_5 (see Fig. 3a and b). We suspect that changing of packing modes between α- and β-ThB_2O_5 is necessary for the large molar volume change (~12%), where there is a similar density increase α to β phase. This is comparable with to the $ThMo_2O_8$ polymorphs, where a large volume change (~20%) for the HT/HP–$ThMo_2O_8$ modification is described compared with its other ambient pressure polymorphs.[19]

3.2.1 Coordination environment and geometry of B and Th centres. Tetravalent Th cations have been observed to possess complex oxygen coordination environments where CNs range from six to fifteen are reported, depending on the type of ligands.[24,25] The connection between Th polyhedra and oxoborate groups produces numerous thorium borate architectures. In the structure of β-ThB_2O_5, B(1)O_4 tetrahedra are found to be face sharing with one, corner sharing with three and edge sharing with one ThO_{8+2} polyhedra, denoted as $ThTh_3BTh$, existing in form of the square pyramid geometry (see Fig. 4a). B(2)O_3 triangles are edge sharing with one and corner sharing with two Th polyhedra, exhibiting a planar triangle geometry as $ThBTh_2$ (see Fig. 4b). ThO_{10} polyhedra are corner, edge and face sharing with five BO_4 tetrahedra and

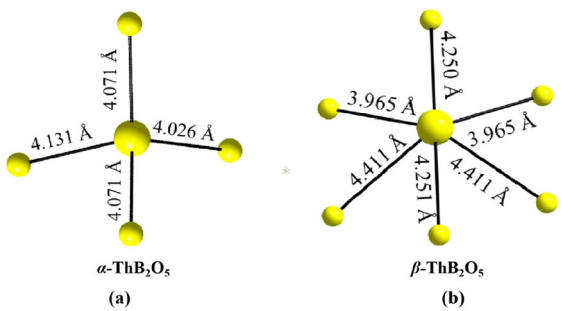

Fig. 3 The adjacent Th–Th bond distances in two polymorphs for α-ThB_2O_5 (a) and β-ThB_2O_5 (b).

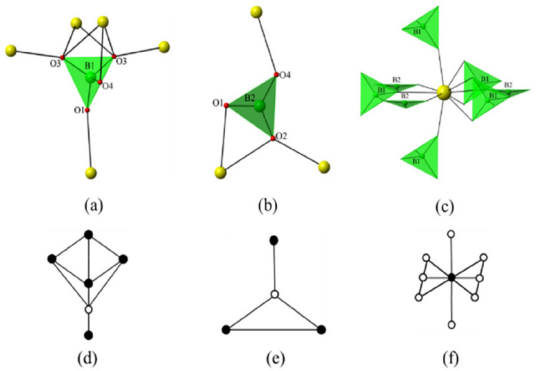

Fig. 4 For β-ThB_2O_5; the coordination environment of a B(1)O_4 tetrahedron (a), coordination environment of a B(2)O_3 triangle (b), coordination environment of ThO_{8+2} polyhedra (c) and the corresponding schematic topological representation of square pyramid geometry (d), schematic topological representation of a trigonal geometry (e), schematic topological representation of a hexagonal bipyramidal shape of Th coordination (f).

three BO_3 triangles, forming a Th-centred hexagonal bipyramidal (ThB_8) geometry (see Fig. 4c). This Th coordination environment is apparently the first reported for inorganic Th bearing compounds. To better observe the Th–Th coordination environments and spatial interactions more clearly, Voronoi–Dirichlet polyhedra (VDP) of Th atoms in Th sub-lattices have been described for both polymorphs of ThB_2O_5 (see Fig. S10†). The Th VDP of β-ThB_2O_5 show a truncated cuboctahedron with the combinatorial–topological type (CTT) of $4^5{\cdot}5^2{\cdot}6^5$. This face distribution symbol means that there are three different numbers (5,2,5) of different (4,5,6) faces. Whereas the CTT of the Th atoms for α-ThB_2O_5 is considerably different, shown as $3^4{\cdot}4^4{\cdot}5^8{\cdot}10^4$ in Fig. S10.† The large differences between CTTs for the Th atoms in the VDP indicate that, Th atoms have a totally different spatial distribution in the two polymorphic modifications.

3.2.2 Structural topology analysis. To examine the cationic topology of the ThB_2O_5 polymorphs, we omitted the anions whilst retaining the connectivity between the cations from the 3D thorium borate framework of β-ThB_2O_5. As shown in Fig. S11,† B1 and B2 are linked along the *a*-axis forming a zigzag B chain⋯B1B2B1B2B1⋯(see Fig. S11a†). Th cations are connected with six other neighboring ones forming a 2D Th layer parallel to the *ab*-plain. Each Th is a [3^6] node within the 2D Th-sheet topology (Fig. S11b†). The zigzag B-chains are bridged over those parallel Th-sheets along the *c*-axis and constructed the 3D ThB_2 framework (see Fig. S11c†). The simplified ThB_2 network can be depicted as a new 3-nodal net topological type with a point symbol of {3^4, 4^{10}, 5^{10}, 6^4}{3^4, 4^{10}, 5^6, 6}{3^4, 4^4, 5^2}.

3.3 Temperature and pressure relationship between α- and β-ThB_2O_5

To understand the temperature and pressure dependence of ThB_2O_5 polymorphs, both were examined using *in situ* powder X-ray diffraction, and under *ex situ* HT/HP conditions (post PXRD examination).

3.3.1 *In situ* HT-PXRD measurement analysis. *In situ* PXRD measurements were made against a pure sample of α-ThB_2O_5 and mixed sample of α- and β-ThB_2O_5 (∼ ratio α/β = 3/1), a mixture sample was chosen to observe which phase would be preferred at higher temperature and to compare the relative change to lattice volume with heating (ESI Fig. S2†). For pure α-ThB_2O_5 PXRD measurements were collected incrementally as the sample was headed towards 1030 °C from RT (Fig. 5) and the data analysed using sequential refinements with the Le Bail method. It can be observed that between 630 and 840 °C reflections corresponding to α-ThB_2O_5 begin sharply changing intensity and positions. From refinement analysis, this region corresponds to non-isotropic thermal expansion where considerable contraction of the *a* parameter occurs whereas the *b*, *c* and *β* parameters showed increased expansion (see ESI Fig. S3†).

Interestingly, continual heating above 840 towards 927 °C further reflections can be observed to occur as can be seen in Fig. 5 but also particularly highlighted in Fig. 6. That these reflections occur independently with respect to the main reflections of β-ThB_2O_5 indicates that the sample is undergoing a discontinuous 1st order phase transformation. This corresponds to the formation of β-ThB_2O_5. The phase transformation motif is further supported when the refined lattice volumes are compared (Fig. S4†). β-ThB_2O_5 is found to occur only over a narrow temperature range as further heating above 1020 °C results in its decomposition. This is supported by TGA measurements performed on α-ThB_2O_5 to 1200 °C (see section below).

3.3.2 Thermogravimetric analysis. TGA measurements were performed in the temperature range of 200–1200 °C (see Fig. S12†). From TGA measurements of a single-phase sample of α-ThB_2O_5 indicated there is no obvious weight loss up to 1200 °C, based on the TG curve (Fig. S12†). TGA-DSC measurements of a single-phase sample of α-ThB_2O_5 indicated a thermal event at ∼630 °C. This is consistent with the onset of the phase transformation observed in the *in situ* PXRD measurements. The DSC curve shows a strong endothermic peak at ∼1053 °C, which corresponds to the decomposition of

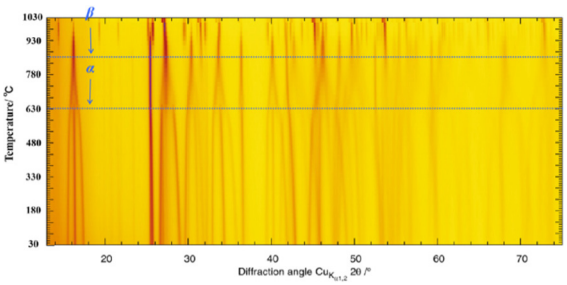

Fig. 5 Temperature dependence of a portion of the PXRD profiles for α-ThB_2O_5 heated from 0 to 1030 °C illustrating the transition from the α to β phase between 807 °C and 927 °C.

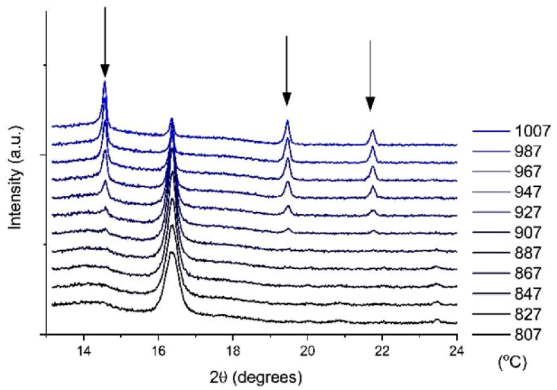

Fig. 6 Portion of PXRD data between 13 and 24° for ThB_2O_5 heated from 807 to 1007 °C. The occurrence of additional reflections above 887 °C (most noticeable at 14.9, 19.5 and 22° as shown by the arrows) indicates a 1st order phase transformation is occurring resulting in β-ThB_2O_5.

the β-phase, which is supported by the *in situ* PXRD results described earlier. The TG-DSC curves, *in situ* PXRD pattern and HT/HP-ThB_2O_5 PXRD pattern are shown in Fig. S12† and Fig. 5, Fig. S2.†

3.3.3 *Ex situ* HT/HP PXRD measurement analysis. To examine the pressure influence on α- and β-phase stability, a mixture of these was treated under HT/HP conditions at 900 °C and 4 GPa and the resulting product analysed with PXRD. Collected PXRD data for the pre- and post-HT/HP α-ThB_2O_5/β-ThB_2O_5 mixtures were analysed using the Rietveld method in the program GSAS-II. The refinement profiles are given in Fig. 7.

For the initial (pre-HT/HP) α-ThB_2O_5/β-ThB_2O_5 mixture monoclinic models in space groups $C2/c$ and $P2_1/m$ could be refined against the PXRD data consistent with α-ThB_2O_5 and β-ThB_2O_5 respectively. An additional ThO_2 impurity phase was also identified, speculated to arise from the initial as synthesised ThB_2O_5. Phase analysis indicated the sample to be 85.6(15), 12.9(6) and 1.48(2) wt% for α-ThB_2O_5, β-ThB_2O_5 and ThO_2 respectively largely consistent with initial experimental input amounts. For the post-HT/HP α-ThB_2O_5/β-ThB_2O_5 mixture, monoclinic and cubic models in space group $P2_1/m$ and $Fm\bar{3}m$ respectively consistent with β-ThB_2O_5 and ThO_2 could be successfully refined against the collected PXRD data. Phase analysis indicates the sample to be 97(1) and 2.3(3) wt% for β-ThB_2O_5 and ThO_2 respectively. From these *ex situ* measurements and analysis, it indicates that the application of HT/HP conditions to the α-ThB_2O_5/β-ThB_2O_5 mix results in the conversion of α-ThB_2O_5 to β-ThB_2O_5, such that β-ThB_2O_5 is the preferred phase under HT/HP conditions. The occurrence of a slightly increased relative amount of ThO_2 is speculated to be related to partial sample decomposition occurring.

3.4 Vibrational spectroscopy

Raman spectrum of β-ThB_2O_5 was measured in the region of 100–1500 cm^{-1}. As shown in Fig. S13,† the modes in low-frequency region from 187–389 cm^{-1} are raised from the lattice

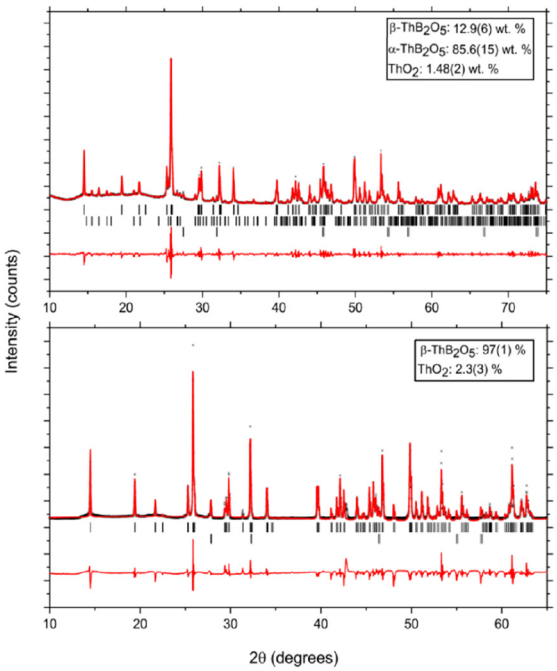

Fig. 7 Rietveld refinements profiles for the α-ThB_2O_5/β-ThB_2O_5 mix pre- (top) and post- (bottom) HT/HP treatment. For top; β-ThB_2O_5 was refined in a monoclinic structure (SG = $P2_1/m$), where a = 4.2400(16) Å, b = 6.8504(7) Å, c = 6.302(3) Å, and β = 106.300(7)°, α-ThB_2O_5 was refined in a monoclinic structure (SG = $C2/c$), where a = 11.548(7) Å, b = 6.9360(20) Å, c = 10.272(6) Å, and β = 101.56(2)°, ThO_2 was refined in a cubic structure (SG = $Fm\bar{3}m$), where a = 5.597(1) Å and where wR = 15.58%. For bottom; β-ThB2O5 was refined in a monoclinic structure (SG = $P2_1/m$), where a = 4.2417(8) Å, b = 6.8549(5) Å, c = 6.3047(19) Å, and β = 106.305(4)°, ThO_2 was refined in a cubic structure (SG = $Fm\bar{3}m$), where a = 5.5304(8) Å, and where wR = 17.60%.

vibrations. The Raman band with a very strong peak around 526 cm^{-1} can be attributed to the bending character ν_4 mode of BO_4 tetrahedra. Raman bands with weak peaks around 800 cm^{-1} are due to the symmetric stretching ν_1 mode of BO_4 units. The Raman band at around 966 cm^{-1} were assigned to the B–O–B symmetrical stretching ν_3 mode in BO_3 triangles. The peaks around 1362 cm^{-1} can be attributed to the doubly degenerate asymmetrical stretching ν_4 mode of the B–O bonds in the trigonal BO_3 units. For α-ThB_2O_5, Raman band with a strong peak at 472 cm^{-1} are attributed to the doubly degenerate in-plane O–B–O bending ν_1 mode from the planar trigonal BO_3 groups. The weak peaks at 700 cm^{-1} and 803 cm^{-1} can be assigned to the B–O bending ν_2 mode in the BO_3 triangles. The symmetrical stretching ν_3 modes of BO_3 groups have caused the peaks at Raman bands of 918 cm^{-1} and 1000 cm^{-1}. The Raman band with a weak peak at 1416 cm^{-1} is attributed to the doubly degenerate asymmetrical stretching ν_4 mode of BO_3 units.[26,27]

IR spectra of both phases were measured in the range of 4000–400 cm^{-1} (see Fig. 8 black curve). The IR spectra of both phases show very high transmittance in the range of 4000–1600 cm^{-1} (2.50–6.25 μm). The absorption bands between 1027 cm^{-1} and 1438 cm^{-1} in both curves can be assigned to the antisymmetric stretching vibrations of the BO_3

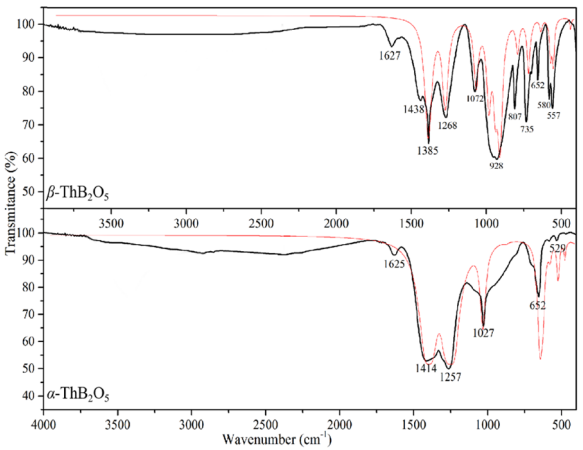

Fig. 8 IR spectra experimental (black) and calculated (red) curves of α-ThB_2O_5 and β-ThB_2O_5.

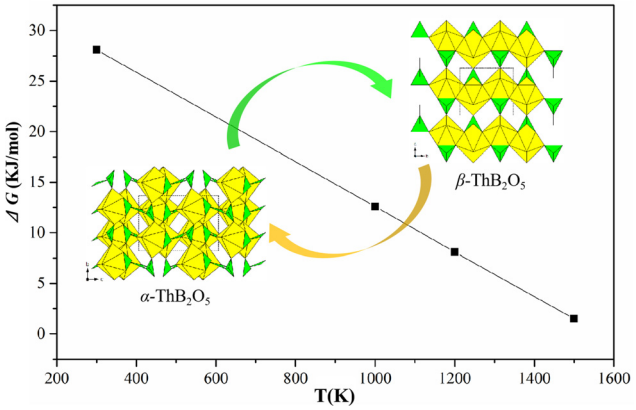

Fig. 9 The computed difference in Gibbs free energy between α-ThB_2O_5 and β-ThB_2O_5 phases. $\Delta G = G(\beta\text{-}ThB_2O_5) - G(\alpha\text{-}ThB_2O_5)$.

groups in the two compounds. The peaks associated with the BO_4 symmetric stretch vibrations appeared in the range of 928–735 cm^{-1} for β-ThB_2O_5. The absorption peaks at 529–652 cm^{-1} can be assigned to bending vibrations of BO_3 and BO_4 groups for α-ThB_2O_5 and BO_3 groups for β-ThB_2O_5. These assignments are consistent with the borates reported previously.[22]

3.5 DFT investigations of α- and β-polymorphs

To understand the thermodynamic stability and spectroscopic properties of studied polymorphic modifications we performed a DFT study of both structures. The computed lattice parameters for the α-ThB_2O_5 and β-ThB_2O_5 phases are reported in Table S3.† The lattice parameters of β-ThB_2O_5 phase are reproduced with surprisingly good accuracy with relative error much smaller than 1% and the volume being off from the experimental value by just 0.6%. On the other hand, the lattice parameters of α-ThB_2O_5 are off the experimental values by up to 1.5% with the volume being overestimated by 2.5%, although this is still reasonably good performance of DFT. Despite these offsets, we notice that both structures are well reproduced, and the DFT-based geometry relaxation did not result in significant deformation of the experimental structures, which were taken as starting configurations. In Table 2 we present the values of relative internal energies (enthalpies) and free energies computed *via* adding vibrational entropy and zero point energy contributions for temperatures of 300K (ambient conditions), 1000 K, 1200 K and 1500 K. The Gibbs free energies are computed as:

$$G = U + \mathrm{ZPE} - ST$$

where U is the internal energy, ZPE is the zero-point energy contribution, S is the vibrational entropy and T is the temperature. We report the differences in Gibbs free energies of the two phases $\Delta G = G(\beta\text{-}ThB_2O_5) - G(\alpha\text{-}ThB_2O_5)$ at selected temperatures (see Fig. 9).

The calculations show that α-ThB_2O_5 phase is the more stable phase at low temperature with the internal energy difference at 0 K of 34.4 kJ mol^{-1}. This is consistent with experimental observation which have been discussed in thermal and *in situ* PXRD analyses section. Increasing the temperature, the free energy difference decreases reaching zero at temperature just above 1500 K.

4. Conclusions

Only the second known polymorph of ThB_2O_5, β-ThB_2O_5, was synthesised from HT/HP conditions and characterised using X-ray single crystal, powder diffraction and spectroscopic methods. The structure of β-ThB_2O_5 is starkly different in comparison to the known α-phase[1] and to the wider family of AB_2O_5 compounds (A = Zr, Hf).[21,22] The β-modification features a dense 3D thorium borate framework, which is composed of [3^6] topological 2D thorium layers on the *ab*-plane and 1D boron–oxygen zigzag chains along the *a*-axis. The structure further possesses tetra-capped trigonal prisms of ThO_{10} polyhedra that are apparently the first observed in inorganic thorium compounds. The previously known α variant with regard to the β, was found to be the lower temperature and lower pressure preferred phase as shown by HT/HP synthesis experiments, *in situ* heating PXRD measurements and supported by *ab initio* calculations. From *in situ* heating PXRD measurements the α polymorph was observed to transform to the β form at approximately 900 °C *via* a 1st order discontinuous phase transformation. β-ThB_2O_5 was found to exist only over a narrow temperature range, decomposing above 1050 °C. Interestingly it was found that by switching fluxes from borax, used to synthesis the α variant under high temperature conditions, to carbonates, the β variant could be synthesised, which was identical to that obtained from HT/HP synthesis. This study demonstrates how subtle changes to synthesis conditions, including temperature, pressure but also and pertinently choice of flux, can dramatically influence different results in structure formation of ThB_2O_5 polymorphs and potentially maybe applicable in synthesis design of other inorganic compounds.

Conflicts of interest

There are no conflicts to declare.

Acknowledgements

Authors are grateful to the Natural Science Foundation of the Education Department of Anhui Province (KJ2019A0831), Hefei University Talent Funding (18-19RC14), Natural Science Foundation of Anhui Province (2008085QB56), HFUU Bilingual Course Construction Project (2021Yyykc02) and Teaching and Research Project of Hefei 2019hfjyxm09. E. V. A. is grateful for DFG for the funding within the AL1527/3-1 project.

References

1 A. Cousson and M. Gasperin, Synthesis and Structure of Thorium Borate: ThB_2O_5, *Acta Crystallogr., Sect. C: Cryst. Struct. Commun.*, 1991, **C47**, 10.

2 J. Arnold, T. L. Gianetti and Y. Kashtan, Thorium lends a fiery hand, *Nat. Chem.*, 2014, **6**, 554.

3 (*a*) D. L. Clark, M. P. Neu, W. Runde and D. W. Keogh, *Kirk-Othmer Encyclopedia of Chemical Technology*, 2006; (*b*) G. L. Murphy, Y. Wang, P. Kegler, Y. Wang, S. Wang and E. V. Alekseev, The first actinide polyiodate: a complex multifunctional compound with promising X-ray luminescence properties and proton conductivity, *Chem. Commun.*, 2021, **57**, 496.

4 (*a*) R. M. Hazen, R. C. Ewing and D. A. Sverjensky, Evolution of uranium and thorium minerals, *Am. Mineral.*, 2009, **94**, 1293; (*b*) G. L. Murphy, P. Kegler, M. Klinkenberg, A. Wilden, M. Henkes, D. Schneider and E. V. Alekseev, Incorporation of iodine into uranium oxyhydroxide phases, *Dalton Trans.*, 2021, **50**, 17257; (*c*) G. L. Murphy, B. J. Kennedy, J. A. Kimpton, Q. Gu, B. Johannessen, G. Beridze, P. M. Kowalski, D. Bosbach, M. Avdeev and Z. Zhang, Nonstoichiometry in Strontium Uranium Oxide: Understanding the Rhombohedral–Orthorhombic Transition in $SrUO_4$, *Inorg. Chem.*, 2016, **55**, 9329.

5 (*a*) W. Stoll, *Ullmann's Encyclopedia of Industrial Chemistry*, 2000; (*b*) G. L. Murphy, C.-H. Wang, G. Beridze, Z. Zhang, J. A. Kimpton, M. Avdeev, P. M. Kowalski and B. J. Kennedy, Unexpected crystallographic phase transformation in non-stoichiometric $SrUO_{4-x}$: Reversible oxygen defect ordering and symmetry lowering with increasing temperature, *Inorg. Chem.*, 2018, **57**, 5948.

6 (*a*) P. C. Burns, The Crystal Chemistry of Uranium in Uranium: Mineralogy Geochemistry and The Environment, in *Reviews in Mineralogy and Geochemistry*, ed. P. C. Burns and R. Finch, Mineralogical Society of America, Washington, D. C., 1999, vol. 38, pp. 23; (*b*) G. L. Murphy, Z. Zhang, R. Tesch, P. M. Kowalski, M. Avdeev, E. Y. Kuo, D. J. Gregg, P. Kegler, E. V. Alekseev and B. J. Kennedy, Tilting and Distortion in Rutile-Related Mixed Metal Ternary Uranium Oxides: A Structural, Spectroscopic, and Theoretical Investigation, *Inorg. Chem.*, 2021, **60**, 2246; (*c*) G. L. Murphy, B. J. Kennedy, Z. Zhang, M. Avdeev, H. E. A. Brand, P. Kegler and E. V. Alekseev, Structure and phase transition in $BaThO_3$: A combined neutron and synchrotron X-ray diffraction study, *J. Alloys Compd.*, 2017, **727**, 1044.

7 (*a*) C. Xiao, A. Khayambashi and S. Wang, Separation and Remediation of $^{99}TcO^{4-}$ from Aqueous Solutions, *Chem. Mater.*, 2019, **31**, 3863; (*b*) L. Jian, K. T. Praveen and S. Denis, Metal–Organic Frameworks for Removal of Xe and Kr from Nuclear Fuel Reprocessing Plants, *Langmuir*, 2012, **28**, 11584; (*c*) S. L. Griffin and N. R. Champness, A periodic table of metal-organic frameworks, *Coord. Chem. Rev.*, 2020, **414**, 213295.

8 B. Xiao, J. Dellen, H. Schlenz, D. Bosbach, E. V. Suleimanov and E. V. Alekseev, Unexpected Structural Complexity in Cesium Thorium Molybdates, *Cryst. Growth Des.*, 2014, **14**, 2677.

9 S. Wang, E. V. Alekseev, J. Diwu, W. H. Casey, B. L. Phillips, W. Depmeier and T. E. Albrecht Schmitt, NDTB-1: A Supertetrahedral Cationic Framework that Removes TcO^{4-} from Solution, *Angew. Chem., Int. Ed.*, 2010, **49**, 1057.

10 E. Hinteregger, T. S. Hofer, G. Heymann, L. Perfler, F. Kraus and H. Huppertz, High-Pressure Synthesis and Characterization of New Actinide Borates, AnB_4O_8 (An = Th, U), *Chem. – Eur. J.*, 2013, **19**, 15985.

11 (*a*) *CrystalClear, version 1.3.5*, Rigaku Corp., Woodlands, TX, 1999; (*b*) G. M. Sheldrick, *SHELXTL, Crystallographic Software Package, version 5.1*, Bruker-AXS, Madison, WI, 1998; (*c*) A. L. Spek, *PLATON*, Utrecht University, Utrecht, The Netherlands, 2001; (*d*) V. A. Blatov and V. N. Serezhkin, Stereoatomic Model of the Structure of Inorganic and Coordination Compounds, *Russ. J. Inorg. Chem.*, 2000, **45**, S105.

12 C. F. Macrae, I. J. Bruno, J. A. Chisholm, P. R. Edgington, P. McCabe, E. Pidcock and P. A. Wood, Mercury CSD 2.0-new features for the visualization and investigation of crystal structures, *J. Appl. Crystallogr.*, 2008, **41**, 466.

13 B. H. Toby and R. B. Von Dreele, GSAS-II: the genesis of a modern open-source all purpose crystallography software package, *J. Appl. Crystallogr.*, 2013, **46**, 544.

14 (*a*) I. D. Brown and D. Altermatt, Bond-valence parameters obtained from a systematic analysis of the inorganic crystal structure database, *Acta Crystallogr., Sect. B: Struct. Sci., Cryst. Eng. Mater.*, 1985, **B41**, 244; (*b*) N. E. Brese and M. O'Keeffe, Bond-valence parameters for solids, *Acta Crystallogr., Sect. B: Struct. Sci., Cryst. Eng. Mater.*, 1991, **B47**, 192.

15 P. Giannozzi, S. Baroni, N. Bonini, M. Calandra, R. Car, C. Cavazzoni, D. Ceresoli, G. L. Chiarotti, M. Cococcioni, I. Dabo, A. Dal Corso, S. de Gironcoli, S. Fabris, G. F. Fratesi, R. Gebauer, U. Gerstmann, C. Gougoussis, A. Kokalj, M. Lazzeri, L. Martin-Samos, N. Marzari, F. Mauri, R. Mazzarello, S. Paolini, A. Pasquarello, L. Paulatto, C. Sbraccia, S. Scandolo, G. Sclauzero,

A. P. Seitsonen, A. Smogunov, P. Umari and R. M. Wentzcovitch, QUANTUM ESPRESSO: a modular and open-source software project for quantum simulations of materials, *J. Phys.: Condens. Matter*, 2009, **21**, 5502.

16 J. P. Perdew, A. Ruzsinszky, G. I. Csonka, O. A. Vydrov, G. E. Scuseria, L. A. Constantin, X. Zhou and K. Burke, Restoring the Density-gradient Expansion for Exchange in Solids and Surfaces, *Phys. Rev. Lett.*, 2008, **100**, 136406.

17 G. Murphy, B. Kennedy, J. Kimpton, Q.-F. Gu, B. Johannesen, G. Beridze, P. M. Kowalski, D. Bosbach, M. Avdeev and Z. Zhang, Nonstoichiometry in Strontium Uranium Oxide: Understanding the Rhombohedral–Orthorhombic Transition in $SrUO_4$, *Inorg. Chem.*, 2016, **55**, 9329.

18 D. Vanderbilt, Soft Self-consistent Pseudopotentials in a Generalized Eigenvalue Formalism, *Phys. Rev. B: Condens. Matter Mater. Phys.*, 1990, **41**, 7892.

19 X. Bin, K. Philip, M. G. Thorsten, R. Lars, A. Kowalski, P. Li, Y. Klepov, V. V. Bosbach, D. Alekseev and E. V, Giant Volume Change and Topological Gaps in Temperature–and Pressure–Induced Phase Transitions: Experimental and Computational Study of $ThMo_2O_8$, *Chem. – Eur. J.*, 2016, **22**, 946.

20 M. Methfessel and A. T. Paxton, High-precision Sampling for Brillouin-zone Integration in Metals, *Phys. Rev. B: Condens. Matter Mater. Phys.*, 1989, **40**, 3616.

21 J. S. Knyrim and H. Huppertz, High-Pressure Synthesis, Crystal Structure, and, Properties of the First Ternary Hafniumborate β-HfB_2O_5, *J. Solid State Chem.*, 2007, **180**, 742.

22 J. S. Knyrim and H. Huppertz, High-pressure Synthesis, Crystal Structure, and, Properties of the First Ternary Zirconium Borate β-ZrB_2O_5, *Z. Naturforsch., B*, 2008, **63**, 707.

23 (*a*) S. Wang, E. V. Alekseev, J. T. Stritzinger, G. Liu, W. Depmeier and T. E. Albrecht-Schmitt, Structure-Property Relationships in Lithium, Silver, and Cesium Uranyl Borates, *Chem. Mater.*, 2010, **22**, 5983; (*b*) Y. Hao, V. V. Klepov, G. L. Murphy, G. Modolo, D. Bosbach, T. E. Albrecht-Schmitt, B. J. Kennedy, S. Wang and E. V. Alekseev, Influence of Synthetic Conditions on Chemistry and Structural Properties of Alkaline Earth Uranyl Borates, *Cryst. Growth Des.*, 2016, **16**, 5923; (*c*) Y. Hao, P. Kegler, D. Bosbach, T. E. Albrecht-Schmitt, S. Wang and E. V. Alekseev, Divergent Structural Chemistry of Uranyl Borates Obtained from Solid State and Hydrothermal Conditions, *Cryst. Growth Des.*, 2017, **17**, 5898; (*d*) Y. Hao, G. L. Murphy, D. Bosbach, G. Modolo, T. E. Albrecht-Schmitt and E. V. Alekseev, Porous Uranyl Borophosphates with Unique three dimensional Open Framework Structure, *Inorg. Chem.*, 2017, **56**, 9311.

24 Y. Li, Z. Weng, Y. Wang, L. Chen, D. Sheng, Y. Liu, J. Diwu, Z. Chai, T. E. Albrecht-Schmitt and S. Wang, Centrosymmetric and chiral porous thorium organic frameworks exhibiting uncommon thorium coordination environments, *Dalton Trans.*, 2015, **44**, 20867.

25 (*a*) Y. Li, Z. Weng, Y. Wang, L. Chen, D. Sheng, J. Diwu, Z. Chai, T. E. Albrecht-Schmitt and S. Wang, Surprising Coordination for Low-valent Actinides Resembling Uranyl (VI) in Thorium(IV) Organic Hybrid Layered and Framework Structures Based on a Graphene-like (6, 3) Sheet Topology, *Dalton Trans.*, 2016, **45**, 918; (*b*) Y. Hao and E. V. Alekseev, Giant Volume Change and Topological Gaps in Temperature–and Pressure–Induced Phase Transitions: Experimental and Computational Study of $ThMo_2O_8$, *Chem. – Eur. J.*, 2016, **22**, 946.

26 (*a*) Y. C. Hao, C. L. Hu, X. Xu, F. Kong and J. G. Mao, $SrGe_2B_2O_8$ and $Sr_3Ge_2B_6O_{16}$: Novel Strontium Borogermanates with Three-Dimensional and Layered Anionic Architectures, *Inorg. Chem.*, 2013, **52**, 13644; (*b*) E. Smith and G. Dent, *Modern Raman spectroscopy: a practical approach*, *John Wiley & Sons*, 2013, 298. K. Nakamoto, A. Part John Wiley & Sons, Inc., 2009; ; (*c*) Y. Hao, L. He, G. Ge, Q. Zhang, N. Luo, S. Huang and E. V. Alekseev, $Mg_3Pt(BO_3)_2O_2$: The First Platinum Borate from the Flux Technique, *J. Solid State Chem.*, 2020, **281**, 121046.

27 (*a*) Y. C. Hao, X. Xu, F. Kong, J. L. Song and J. G. Mao, $PbCd_2B_6O_{12}$ and $EuZnB_5O_{10}$: syntheses, crystal structures and characterizations of two new mixed metal borates, *CrystEngComm*, 2014, **16**, 7689; (*b*) G. Barros, E. N. Silva, A. P. Ayala, I. Guedes, C. K. Loong and J. Y. Wang, Raman spectroscopic characterization of $RECa_4O(BO_3)$(RE=La and Gd) crystals, *Vib. Spectrosc.*, 2008, **46**, 100; (*c*) Y. Hao, V. V. Klepov, P. Kegler, G. Modolo, D. Bosbach, T. E. Albrecht-Schmitt, S. Wang and E. V. Alekseev, Synthesis and Study of the First Zeolitic Uranium Borate, *Cryst. Growth Des.*, 2017, **18**, 498; (*d*) S. Wang, E. M. Villa, J. Diwu, E. V. Alekseev, W. Depmeier and T. E. Albrecht-Schmitt, Role of Anions and Reaction Conditions in the Preparation of Uranium(VI), Neptunium(VI), and Plutonium(VI) Borates, *Inorg. Chem.*, 2011, **50**, 2527.